Hard Magnetic Materials

Micromagnetic Simulation of Coercivity of Alnico Magnets

Hoyun Won[1], Yang-Ki Hong[1], Minyeong Choi[1], Feng Yan[2], Gary J. Mankey[3], Xiao Han[2], Woncheol Lee[4], Chang-Dong Yeo[5], Jongkook Lee[6], and Taegyu Lee[6]

[1]*Department of Electrical and Computer Engineering, The University of Alabama, Tuscaloosa, AL 35487, USA*
[2]*Department of Metallurgical and Materials Engineering, The University of Alabama, Tuscaloosa, AL 35487, USA*
[3]*Department of Physics and Astronomy, The University of Alabama, Tuscaloosa, AL 35487, USA*
[4]*RF Product Development Group, Samsung Electro-Mechanics Company Ltd., Suwon-si 16674, South Korea*
[5]*Department of Mechanical Engineering, Texas Tech University, Lubbock, TX 79409, USA*
[6]*Institute of Fundamental and Advanced Technology, Hyundai Motor Company, Uiwang-si 16082, South Korea*

Received 11 May 2021, accepted 25 May 2021, published 28 May 2021, current version 2 Jul 2021.

Abstract—A branch connecting two neighboring ferromagnetic α_1-phase rods is one of the geometric factors that contributes to degradation of alnico's normally high coercivity. This letter investigates the effects of various branch geometries and dimensions on the coercivity of alnico comprehensively by using a micromagnetic simulator when the branch is assumed to be connected in either H- or U-shaped alnico structure and the magnetization reversal of the ferromagnetic α_1-phase rod occurs by quasi-coherent rotation or curling. For the H-shaped structure, high coercivity is realized by adopting the middle-branch-connected (MBC) structure with a long branch length and width for quasi-coherent rotation, regardless of the branch thickness. For curling, the same geometric parameters are suggested except for a thick branch thickness. For the U-shaped structure with quasi-coherent rotation, a short branch thickness, width, and length, and MBC position lead a high coercivity. For curling, a short branch width but long length and edge-bridge-connected position result in a high coercivity, regardless of the branch thickness.

Index Terms—Hard magnetic materials, micromagnetic models, magnetic alloys.

I. INTRODUCTION

Rare earth (**RE**)-free-based permanent magnets (**PMs**) have received significant attention due to the hefty price fluctuations and unstable supply of RE minerals, such as neodymium, dysprosium, and terbium [Zhou 2014a, Sun 2015, Zhu 2017]. Among the reported RE-free PMs, alnico PMs show the most promising potential owing to their high saturation magnetization (M_s), high Curie temperature (T_C), and small temperature coefficient of M_s (α) [Zhu 2017]. However, its relatively low intrinsic coercivity (H_{ci}) has limited wide adoption in various applications.

The H_{ci} of alnico is dominantly attributed to the shape anisotropy associated with high-aspect-ratio FeCo-rich rods (α_1-phase) embedded in a nonmagnetic Al-Ni-rich matrix (α_2-phase). One reason for a low H_{ci} of alnico is the α_1-phase branch connecting neighboring ferromagnetic rods [Zhou 2014a, Sun 2015, Zhu 2017]. Ke [2017] simulated the shape of the branch-connected α_1-phase rods as H and U shapes for H_{ci}, as shown in Fig. 1(a) and (b). These two shapes were experimentally observed, as shown in Fig. 2 [Zhou 2014b, Ke 2017]. Accordingly, the micromagnetic simulation was used to investigate the effect of the branch position on each shape's H_{ci} when the magnetization vectors within the α_1-phase rod experience only curling. Analysis of the results concluded that the branch positioned on the bottom of the α_1-phase rod, namely the U-shape, leads to a low H_{ci}. In contrast, the simulation results show that a branch in the middle of the α_1-phase rod, namely the H-shape, does not degrade H_{ci}. Other

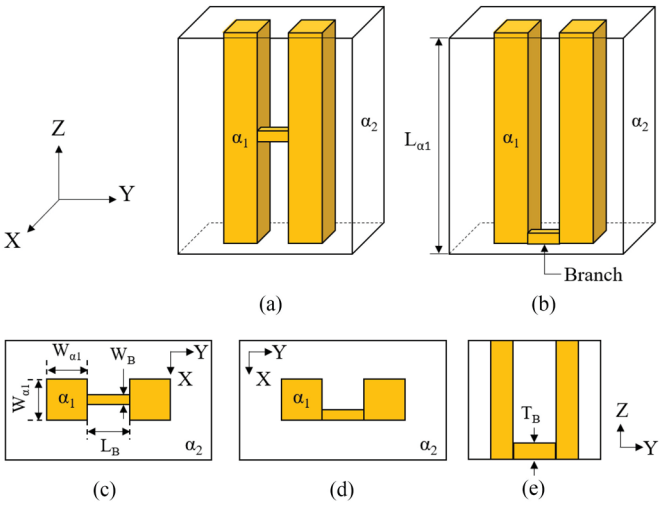

Fig. 1. Overall view of (a) H-shaped and (b) U-shaped structure, top view of (c) MBC and (d) EBC, and (e) side view of the U-shaped structure where $L_{\alpha 1}$ is the α_1-phase rod length, $W_{\alpha 1}$ denotes the α_1-phase rod width, and W_B, L_B, and T_B are the branch width, length, and thickness, respectively.

than these results, there are no other geometric branch parameters studied for alnico's H_{ci}.

Despite the significant impact of the branch on the H_{ci} of alnico, there is no comprehensive study on the effects of nanogeometric parameters on H_{ci} to give insight into the branch's role. Thus, we have investigated the effects of branch geometry and dimension on H_{ci} using a micromagnetic simulation with scenarios where the magnetization vectors within

Corresponding author: Yang-Ki Hong (e-mail: ykhong@eng.ua.edu).
Digital Object Identifier 10.1109/LMAG.2021.3084899

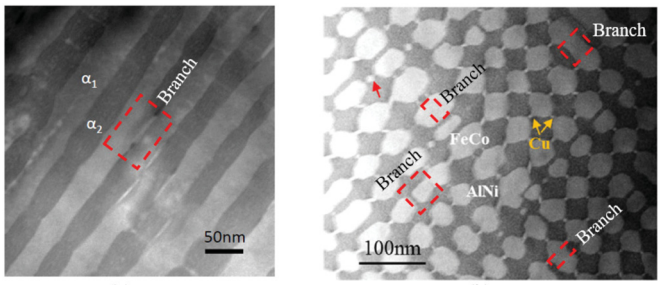

Fig. 2. High-angle annular dark field scanning transmission electron microscopy image of (a) side and (b) top view of alnico [Zhou 2014b, Ke 2017].

the α_1-phase rod exhibit either quasi-coherent rotation or curling. The branch geometric parameters include the branch thickness (T_B), width (W_B), and length (L_B) for two different branch positions along the cross section of the H- and U-shaped structures. The branch positions are the middle-branch-connected (**MBC**) and edge-bridge-connected (**EBC**) structures.

II. MICROMAGNETIC SIMULATION SETUP

Fig. 1 shows H- and U-shaped α_1-phase rectangular rods embedded in the nonmagnetic α_2-phase matrix used to estimate H_{ci}. Micromagnetic computer simulation using an LLG Micromagnetic Simulator v2.63b (developed by M. R. Scheinfein) was performed on both H- and U-shaped alnico to construct magnetic hysteresis loops and thereby H_{ci}, map the detailed magnetic spin configurations, and compute the free energies. The branch geometric parameters for the simulation include T_B, W_B, L_B, and branch position. The magnetic element (α_1-phase rod) and nonmagnetic matrix (α_2-phase) are divided into 1 nm × 1 nm × 2 nm sized cells and simulated with 1 Oe field step for magnetic hysteresis loops. M_s of 1.67×10^6 and exchange stiffness (A) of 1.1×10^{-11} J/m for the α_1-phase and M_s of 0 A/m and A of 0 J/m for the α_2-phase were used in the simulation [Ke 2017]. The α_1-phase rod length ($L_{\alpha 1}$) is set to 200 nm.

Two different α_1-phase rod widths ($W_{\alpha 1}$) were used to study the effects of branch geometry on H_{ci} when the α_1-phase rod experiences either quasi-coherent rotation or curling. The curling occurs in a rectangular rod due to a large demagnetization field in the two ends of the rod. However, the spins in the rod which rotate uniformly because of the small rod width, like the spins in the circular rod which rotate uniformly when its diameter is below the coherent radius. It is reported that when the diameter of the rod is below its coherent radius of 12.8 nm, the magnetic spins within the α_1-phase rod rotate coherently as the applied field changes [Zhou 2014a]. Accordingly, 10 and 25 nm of $W_{\alpha 1}$ are chosen for quasi-coherent rotation and curling, respectively. The simulation shows that the quasi-coherent rotation occurs for the $W_{\alpha 1}$ of 10 nm, as shown in Fig. 3. The following branch geometric parameters are used for simulating both H- and U-shaped structures for H_{ci}.

1) Branch thickness (T_B) ranging from 15 to 125 nm at branch length (L_B) of 15 nm and branch width (W_B) of 60% of α_1-phase rod width ($W_{\alpha 1}$).

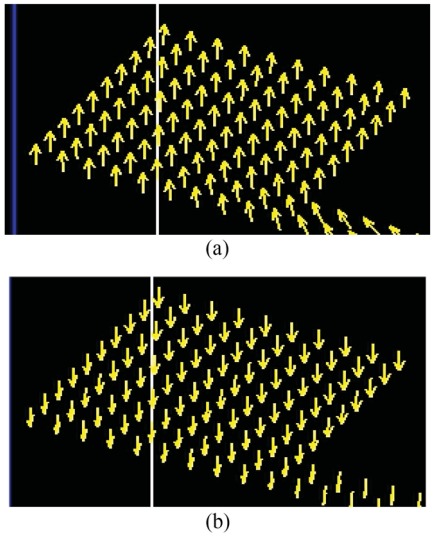

Fig. 3. Surface spin configuration of H-shaped structure with $W_{\alpha 1}$ of 10 nm, T_B of 30 nm, L_B of 15 nm, W_B of 2 nm, and edge-branch-connected position when the applied field is (a) –5.936 kOe and (b) –5.937 kOe.

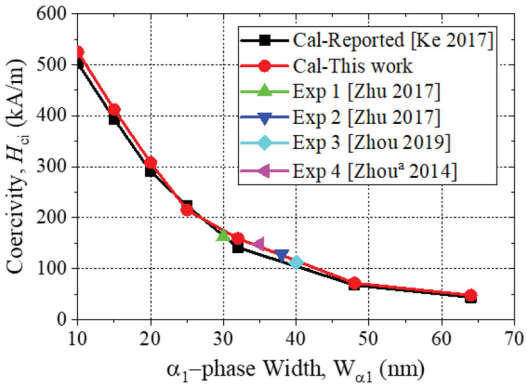

Fig. 4. Intrinsic coercivity versus α_1-phase width ($W_{\alpha 1}$) from literature and simulation.

2) W_B ranging from 20% to 80% of $W_{\alpha 1}$ at L_B of 15 nm and T_B of 30 nm.
3) L_B ranging from 10 to 20 nm at T_B of 30 nm and W_B of 60% of $W_{\alpha 1}$.
4) Branch position, which is MBC or EBC position, as shown in Fig. 1(c) and (d) at 30 nm T_B and 15 nm L_B.

III. RESULTS AND DISCUSSION

First, we simulated the alnico structure without a branch for H_{ci}. The simulated H_{ci} is compared with the H_{ci} at various $W_{\alpha 1}$ simulated using the MuMax3 micromagnetic simulation package [Ke 2017] and the experimental H_{ci} [Zhou 2014a, 2019, Zhu 2017]. Fig. 4 shows the reported and simulated H_{ci} as a function of $W_{\alpha 1}$ ranging from 10 to 64 nm. Our simulated H_{ci} is in good agreement with the average value of the reported H_{ci} of the single rectangular and ellipsoidal rods and the experimental H_{ci}. A decrease of H_{ci} with increasing $W_{\alpha 1}$ can be described by the experimentally verified following equation [Ke

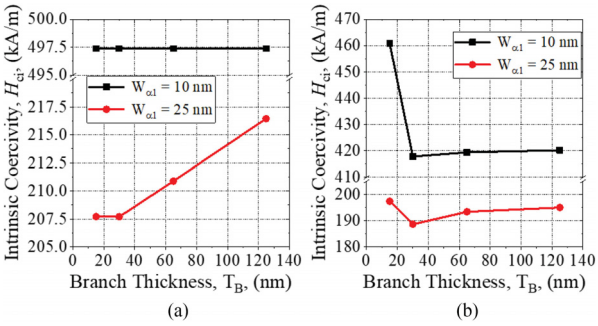

Fig. 5. Intrinsic coercivity versus branch thickness (T_B) for (a) H- and (b) U-shaped alnico with branch width (W_B) of 60% of $W_{\alpha1}$ and 15 nm L_B.

2017]:

$$H_{ci} = 2K_1/(\mu_0 M_s) - c(N_{||})A/(\mu_0 M_s L_{\alpha1}^2) \quad (1)$$

where K_1 is the magnetocrystalline anisotropy constant, $N_{||} \approx 0$ is the demagnetizing factor parallel to each rod's long axis, and the value of $c(N_{||})$ is 6.678 for a needle. With all variables except for the $W_{\alpha1}$ constant in (1), H_{ci} is inversely proportional to the square of the $W_{\alpha1}$.

For our simulations, we varied branch geometric parameters of the H- and U-shaped alnico to comprehensively investigate dimension-dependent H_{ci}. The simulation results show that the H_{ci} of the H-shaped alnico is higher than that of the U-shaped one for all $W_{\alpha1}$, T_B, W_B, L_B, and branch positions. This high H_{ci} is consistent with the results in Ke [2017]. The high H_{ci} is attributed to the magnetization reversal starts at the rod ends [Ke 2017]. This reversal requires less energy for the U-shaped structure than the H-shaped structure, therefore, lowering H_{ci}. The effects of individual geometric parameter on H_{ci} are reported in the following sections.

A. Branch Thickness (T_B)

Fig. 5 shows the effect of T_B on H- and U-shaped alnicos' H_{ci}. Both alnicos have W_B (60% of $W_{\alpha1}$) and 15 nm L_B at 10 nm (quasi-coherent rotation) and 25 nm (curling) $W_{\alpha1}$.

For the H-shaped alnico with 10 nm $W_{\alpha1}$, H_{ci} remains constant at 497.4 kA/m regardless of the T_B. In contrast, when $W_{\alpha1}$ increases to 25 nm, the H_{ci} increases slightly from 207.7 to 223.6 kA/m as the T_B increases from 15 to 125 nm. This increase is because a thicker branch prevents the edge's spins from rotating in a curling mode. As illustrated in Fig. 6, the H-shaped alnico's spin direction with thicker T_B (125 nm) points more upward, i.e., the out-of-plane direction, than the H-shaped alnico with thinner T_B (15 nm). The same trend is observed for other W_B and L_B.

For the U-shaped alnico with 10 nm $W_{\alpha1}$ in Fig. 5(b), H_{ci} first decreases to 417.8 from 460.8 kA/m as the T_B increases to 30 nm from 15 nm and then slightly increases from 417.8 to 419.4 kA/m beyond 30 nm. When $W_{\alpha1}$ increases to 25 nm, a similar H_{ci} behavior is observed. The H_{ci} first decreases to 188.6 from 198.9 kA/m as the T_B increases to 30 from 15 nm and then slightly increases to 194.2 from 188.6 kA/m beyond 30 nm. The H_{ci} decrease between 15 and 30 nm of T_B at both $W_{\alpha1}$ is attributed to a 20%–30.5% increment in the exchange energy (E_{ex}).

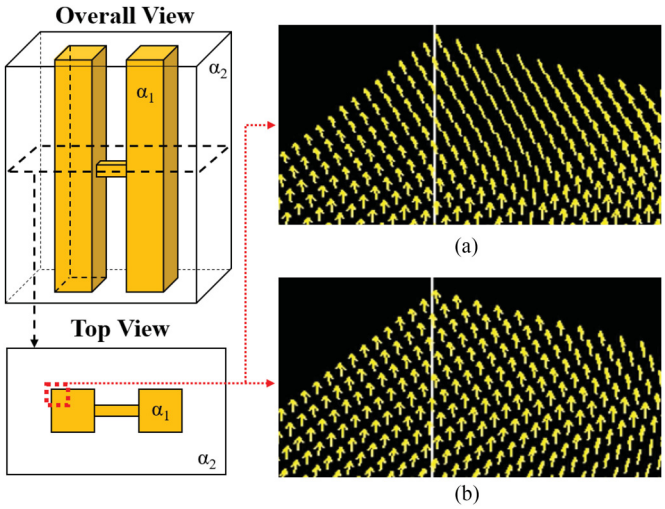

Fig. 6. (Left) Surface spin configuration of top edge of the H-shaped alnico with 25 nm $W_{\alpha1}$, 15 nm L_B, 15 nm W_B, MBC-position, and (a) 15 nm T_B and (b) 125 nm T_B.

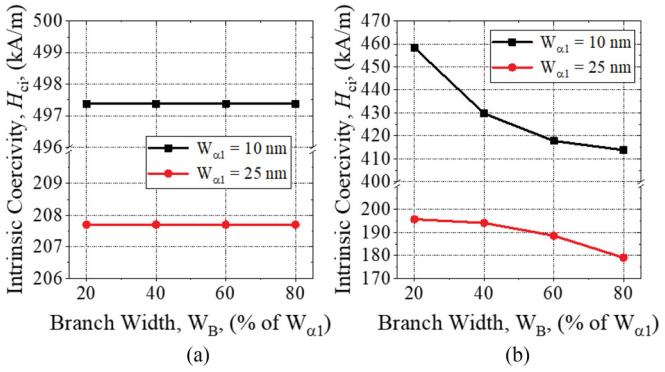

Fig. 7. Intrinsic coercivity versus branch width (W_B) for (a) H- and (b) U-shaped alnico with 15 nm L_B and 30 nm T_B.

While any T_B of H-shaped alnico is suggested for quasi-coherent rotation, thick T_B is recommended for curling. For the U-shaped structure, thin T_B is indicated for both magnetization reversals (quasi-coherent rotation and curling) to realize a high H_{ci}.

B. Branch Width (W_B)

Fig. 7 shows the effects of W_B on H- and U-shaped alnicos' H_{ci}, having 15 nm L_B and 30 nm T_B, at 10 and 25 nm $W_{\alpha1}$. The H-shaped alnico's H_{ci} remains constant at 497.4 kA/m at 10 nm $W_{\alpha1}$ and 207.7 kA/m at 25 nm $W_{\alpha1}$ regardless of W_B. In contrast, the U-shaped alnico's H_{ci} gradually decreases from 458.4 to 417.8 kA/m at 10 nm $W_{\alpha1}$ and 195.8 to 176.7 kA/m at 25 nm $W_{\alpha1}$ as the W_B increases. This decrease is attributed to a significant increase in the exchange energy (E_{ex}) with the W_B, not reported here.

It is noted that while the H_{ci} is unaffected by the W_B for the H-shaped alnico, narrow W_B for both $W_{\alpha1}$ is beneficial for the U-shaped alnico to obtain a high H_{ci}.

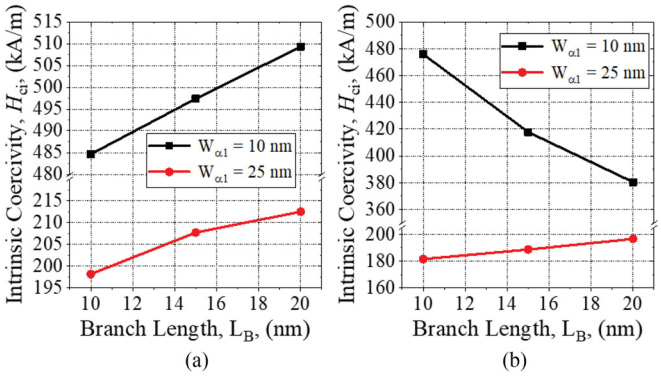

Fig. 8. Intrinsic coercivity versus branch length (L_B) for (a) H- and (b) U-shaped alnico with 30 nm T_B and branch width (W_B) of 60% of $W_{\alpha1}$.

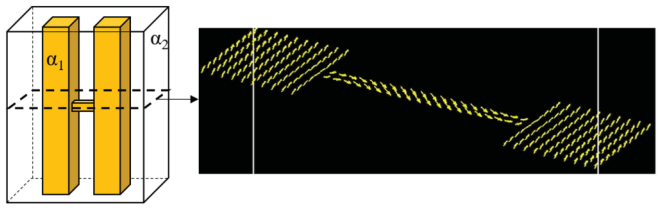

Fig. 9. Surface spin configuration of H-shaped alnico with 10 nm $W_{\alpha1}$, 30 nm T_B, 20 nm L_B, MBC-position, and 2 nm W_B.

C. Branch Length (L_B)

Both H- and U-shaped alnicos with $W_{\alpha1}$ of 10 and 25 nm are simulated for H_{ci} when T_B and W_B are 30 nm and 60% of $W_{\alpha1}$, respectively. Fig. 8 shows the L_B-dependent H_{ci} for H- and U-shaped alnico magnets. As the L_B increases from 10 to 20 nm, the H-shaped alnico's H_{ci} increases from 485.4 to 509.3 kA/m and 198.9 to 212.5 kA/m for 10 nm and 25 nm $W_{\alpha1}$, respectively. Higher H_{ci} for 20 nm L_B than 10 nm at 10 nm $W_{\alpha1}$ is attributed to the branch's in-plane surface spin configuration, as shown in Fig. 9. These results from an external magnetostatic field energy decrease, i.e., lowering the total system energy (E_{tot}).

In contrast, the U-shaped alnico's H_{ci} decreases rapidly as increasing L_B at 10 nm $W_{\alpha1}$ but slightly increases at 25 nm $W_{\alpha1}$. The rapid H_{ci} decrease is mainly attributed to a 54.6% increase in E_{ex} and a 22.93% increase in demagnetization energy (E_{demag}).

The simulation results show that a large L_B for the H-shaped alnico is beneficial to achieve high H_{ci} for both quasi-coherent rotation and curling. Also, a shorter L_B for quasi-coherent rotation and a longer L_B for curling are required for U-shaped alnico.

D. Branch Position

The effects of two branch positions, i.e., MBC and EBC positions in Fig. 1(c) and (d), on alnico's H_{ci} were studied. The L_B and T_B are set to 15 and 30 nm, respectively. Fig. 10 shows H_{ci} as a function of W_B at 10 or 25 nm $W_{\alpha1}$ for H- and U-shaped alnico magnets. For both shapes with 10 nm $W_{\alpha1}$, the MBC positioned alnico shows higher H_{ci} than the EBC one regardless of W_B, as shown in Fig. 10(a) and (b). This high H_{ci} can be understood by the branch's spin configurations. Fig. 11 indicates that the branch's surface spins are in the out-of-plane

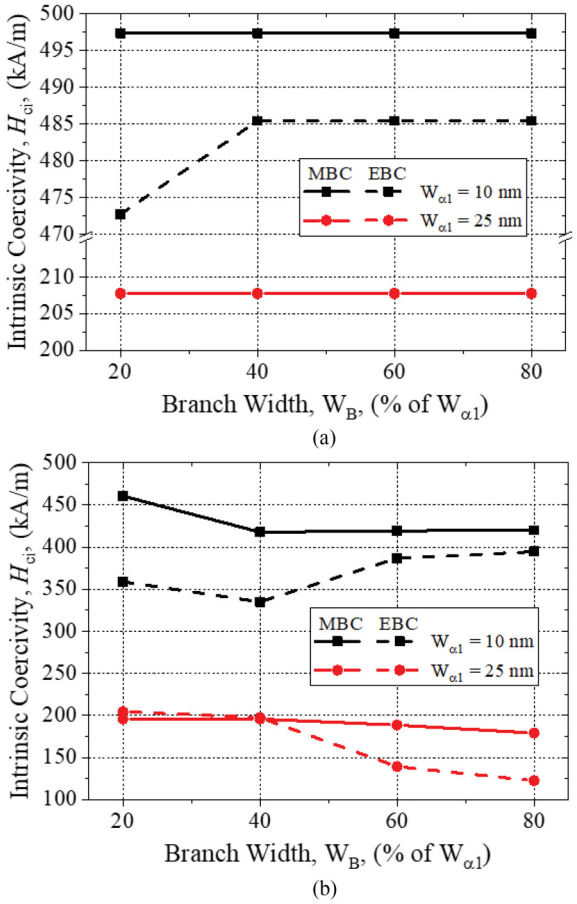

Fig. 10. Intrinsic coercivity versus branch width (W_B) and position for (a) H- and (b) U-shaped alnico with 30 nm T_B and L_B 15 nm.

Table 1. Recommended Branch Design Parameters of H- and U-Shaped Alnico for High H_{ci}

Parameter	H-shaped Structure		U-shaped Structure	
	Quasi-coherent Rotation ($W_{\alpha1}$ = 10 nm)	Curling ($W_{\alpha1}$ = 25 nm)	Quasi-coherent Rotation ($W_{\alpha1}$ = 10 nm)	Curling ($W_{\alpha1}$ = 25 nm)
Branch thickness, T_B	Any	Thick	Thin	Any
Branch width, W_B	Any	Any	Short	Short
Branch length, L_B	Long	Long	Short	Long
Bridge Position	MBC	Any	MBC	EBC

for the MBC structure but in the in-plane spin configuration for the EBC structure.

When the $W_{\alpha1}$ increases to 25 nm, there is no difference in the H_{ci} between MBC and EBC positioned H-shaped alnico magnets, as shown in Fig. 10(a). Regardless of W_B, H_{ci} remains constant at 206.9 kA/m. In contrast, two different trends are noticed for the U-shaped alnico. First, the alnico with the EBC position shows 1.59–8.75 kA/m higher

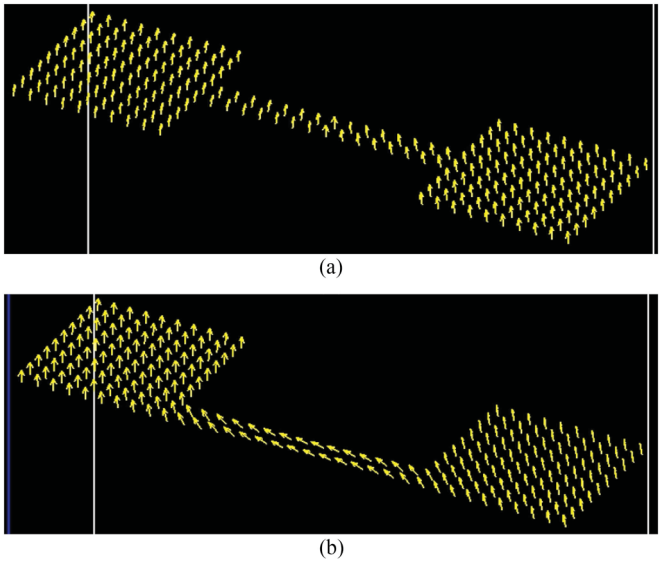

Fig. 11. Surface spin configuration of H-shaped structure with 10 nm $W_{\alpha 1}$, 30 nm T_B, 15 nm L_B, 2 nm W_B, and (a) MBC position and (b) EBC position.

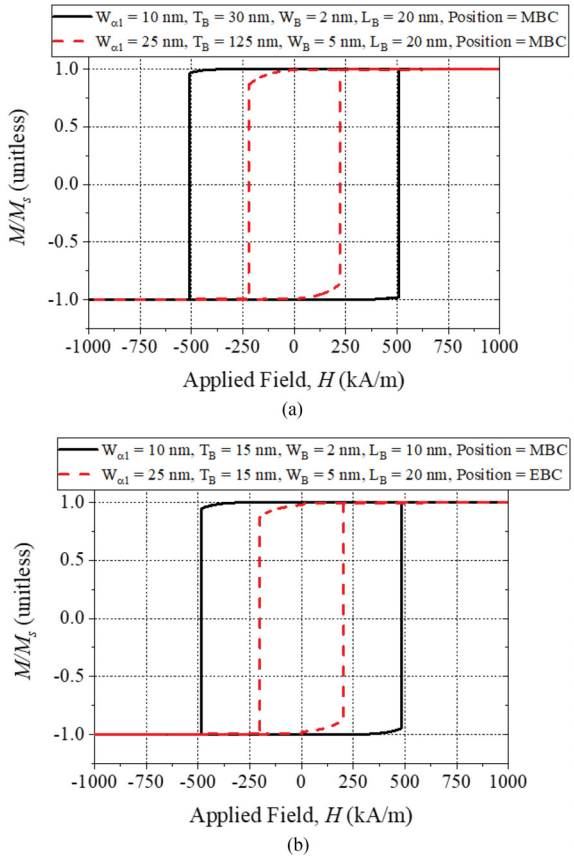

Fig. 12. Normalized M–H hysteresis loop for (a) H- and (b) U-shaped alnico that exhibit highest H_{ci}.

H_{ci} than the alnico with the MBC position until W_B reaches 40% of $W_{\alpha 1}$. However, as the W_B increases to 80% of $W_{\alpha 1}$, the MBC-positioned alnico shows much higher H_{ci} than the EBC-positioned one. The lower H_{ci} with the wider W_B is attributed to the larger branch area allowing spin reversal with a curling spin configuration.

We have optimized the branch geometry and dimension for H- and U-shaped alnico magnets for the highest H_{ci} For H-shaped alnico, highest H_{ci} of 509.3 kA/m is realized with the MBC structure, having 30 nm T_B, W_B of 20% of $W_{\alpha 1}$, and 20 nm L_B when the α_1-phase rod experiences quasi-coherent rotation. For H-shaped alnico rod experiencing curling, the MBC structure having 125 nm T_B, W_B of 20% of $W_{\alpha 1}$, and 20 nm L_B exhibits the highest H_{ci} of 222.8 kA/m. For the U-shaped alnico rod experiencing quasi-coherent rotation, the MBC structure having 15 nm T_B, W_B of 20% of $W_{\alpha 1}$, and 10 nm L_B exhibits a high H_{ci} of 485.4 kA/m, whereas for the rod with the curling, the EBC structure with 15 nm T_B, W_B of 20% of $W_{\alpha 1}$, and 15 nm L_B shows a high H_{ci} of 206.9 kA/m. We used the optimized design parameters in constructing magnetic hysteresis loops, as shown in Fig. 12. The recommended branch design parameters for high H_{ci} are summarized in Table 1.

IV. CONCLUSION

We optimized the branch dimensions of H- and U-shaped alnico magnets using micromagnetic simulation for the cases of quasi-coherent rotation and curling of the ferromagnetic α_1-phase rod to realize high coercivity (H_{ci}). For the H-shaped structure, the MBC structure with a long branch length (L_B) regardless of branch thickness (T_B) and branch width (W_B) realizes high H_{ci} for quasi-coherent rotation. For curling, the same branch dimensions except for a thick T_B are suggested. For the U-shaped structure, thin T_B, short W_B, short L_B, and MBC position are suggested for quasi-coherent rotation, and short W_B, long L_B, and EBC position regardless of T_B for curling are recommended to obtain high H_{ci} of 485.4 and 206.9 kA/m, respectively.

ACKNOWLEDGMENT

This work was supported by the National Science Foundation under Grant 1650564.

REFERENCES

Ke L, Skomski R, Hoffmann T, Zhou L, Tang W, Johnson D, Kramer M, Anderson I, Zhang C (2017), "Simulation of alnico coercivity," *Appl. Phys. Lett.*, vol. 111, 022403, doi: 10.1063/1.4992787.

Sun Y, Zhao Z, Liu Z, Xia W, Zhu S, Lee D, Yan A (2015), "The phase and microstructure analysis of alnico magnets with high coercivity," *J. Magn. Magn. Mater.*, vol. 379, pp. 58–62, doi: 10.1016/j.jmmm.2014.12.003.

Zhou L, Miller M, Lu P, Ke L, Skomski R, Dillon H, Xing D, Palasyuk A, McCartney M, Smith D, Constantinides S, McCallum R, Anderson I, Antropov V, Kramer M (2014a), "Architecture and magnetism of alnico," *Acta Mater.*, vol. 74, pp. 224–233, doi: 10.1016/j.actamat.2014.04.044.

Zhou L, Miller M, Dillon H, Palasyuk A, Constantinides S, McCallum R, Anderson I, Kramer M (2014b), "Role of the applied magnetic field on the microstructural evolution in alnico 8 alloys," *Metall. Mater. Trans. E*, vol. 1, pp. 27–35, doi: 10.1007/s40553-013-0004-3.

Zhou L, Emma W, Ke L, Cullen D, Lu P, Constantinides S, McCallum R, Anderson I, Kramer M (2019), "Microstructure and coercivity in alnico 9," *J. Magn. Magn. Mater.*, vol. 471, pp. 142–147, doi: 10.1016/j.jmmm.2018.09.085.

Zhu S, Zhao J, Xia W, Sun Y, Peng Y, Fu J (2017), "Magnetic structure and coercivity mechanism of AlNiCo magnets studied by electron holography," *J. Alloy Compd.*, vol. 720, pp. 401–407, doi: 10.1016/j.jallcom.2017.05.210.